Soft Matter

RSC Publishing

PAPER

View Article Online
View Journal | View Issue

Geometrical edgeactants control interfacial bending rigidity of colloidal membranes†

Cite this: *Soft Matter*, 2013, **9**, 8306

Mark J. Zakhary, Prerna Sharma, Andrew Ward, Sevim Yardimici and Zvonimir Dogic*

A colloidal membrane is a one rod-length thick monolayer of aligned rods which spontaneously assembles in a mixture of rod-like viruses and non-adsorbing polymer. The complex structure of the monolayer edge modifies its fluctuations, effectively smoothing out the interface. We demonstrate that long filaments such as F-actin or flagella preferentially dissolve in the membrane's edge and can be used to control its interfacial properties. This effect is not driven by energetic interactions, but is rather a direct consequence of the intrinsic geometry of the constituent particles; hence we call such filaments geometrical edgeactants. Using optical manipulation techniques we adsorb individual filaments onto the edge of the colloidal membrane and measure their influence on the edge fluctuations. Edgeactants stiffen the interface, increasing its bending rigidity by up to an order of magnitude. Furthermore, they also locally suppress a polymorphic transition into twisted ribbons inherent to colloidal membranes. These results demonstrate new ways to control soft materials in which the final structure is only determined by the geometry of the constituent objects.

Received 20th March 2013
Accepted 11th June 2013

DOI: 10.1039/c3sm50797a

www.rsc.org/softmatter

1 Introduction

The boundary between two immiscible liquids continuously fluctuates in length as molecules exchange between the bulk suspension and the interface. Such fluctuations are governed by surface tension, the energetic cost associated with taking molecules from the bulk phase and placing them at an interface.[1] In principle, it is also possible for interfaces to have a finite bending rigidity, although in most systems such a term does not seem to be significant. The same interfacial free energy that describes conventional mixtures at the molecular scale also governs fluctuations of phase-separated colloidal systems. In comparison to molecular interfaces, which are roughened on Angstrom lengthscales,[2] the large lengthscale associated with colloidal systems makes it possible to directly visualize their interfacial fluctuations in real space, greatly facilitating quantitative analyses.[3,4] Such experiments have shown that similar to molecular systems, bending rigidity does not play a significant role in dynamics of colloidal interfaces. Replacing spheres with rod-like particles significantly increases the complexity of the phase diagram and leads to formation of more complex interfaces that contain partially ordered liquid crystalline states.[5–14] Besides 3D liquid crystalline droplets, rod-like particles can also assemble into flat 2D colloidal membranes consisting of a liquid-like monolayer of aligned rods.[15,16] The edges of these membranes exhibit dynamics that are easily visualized in real-space, allowing for quantitative measurement of their fluctuation spectra, which are significantly more complex when compared to those of conventional interfaces.[17] Specifically, fluctuations at small wavelengths are suppressed indicating that membrane edges have finite bending rigidity.

Molecular interfaces can be modified by addition of amphiphilic surfactants which, being insoluble in either bulk phase, preferentially dissolve at an interface and thus modify its surface tension. Here, we study the behavior of colloidal membranes in the presence of a low concentration of semi-flexible filaments, which serve as edge-active agents, or edgeactants. Long filaments, such as F-actin or bacterial flagella, are insoluble in both the virus-rich colloidal membranes and polymer-rich isotropic phase. Instead, they preferentially dissolve into the quasi-one-dimensional nematic phase associated with the edge of colloidal membranes. Unlike conventional surfactants which are driven to the surface by effective energetic interactions, filament adsorption onto the membrane's edge is entirely due to geometric considerations. These geometrical edgeactants can be directly manipulated owing to their colloidal nature, allowing us to sequentially add single filaments to the membrane edge while simultaneously determining their effect on the interfacial fluctuations. Unlike molecular amphiphilic surfactants which primarily control the magnitude of the interfacial tension, the predominant effect of geometrical edgeactants is to modify the bending rigidity of the 1D interface associated with the membrane edge.

The rest of this paper is organized as follows. We first review the molecular forces that drive assembly of colloidal membranes.

Department of Physics, Brandeis University, Waltham, MA 02453, USA. E-mail: zdogic@brandeis.edu

† Electronic supplementary information (ESI) available. See DOI: 10.1039/c3sm50797a

Subsequently, we describe experiments which quantify the fluctuations of the interface with predetermined numbers of edge-bound filaments. We demonstrate wide applicability of our method by using filaments whose bending rigidities differ by orders of magnitude. Finally, we demonstrate that the presence of edgeactants locally suppresses the polymorphic disk-to-ribbon transition which is inherent to colloidal membranes assembled from chiral rods.[17] These findings outline the possibility of engineering edgeactants with more complex shapes in order to assemble colloidal membranes of finite size, analogous to molecular microemulsions.

2 Interfacial properties of colloidal membranes

2.1 Structure and fluctuations of colloidal membranes

For assembly of colloidal membranes we use *fd*, an 880 nm rod-like bacteriophage with a diameter of 6 nm and a persistence length of 2.8 μm.[25] Nature has engineered these viruses to be essentially identical to each other, making it possible to prepare large-scale suspensions of much higher monodispersity when compared to most synthetic rod-like colloids. *fd* viruses are mixed with the non-adsorbing polymer dextran (M_w 500 000), whose effective radius of gyration in aqueous solvent is 17 nm.[19] Polymer coils exert a uniform osmotic pressure on isolated rod-like viruses in solution. When two viruses approach each other, however, the depleting polymer is excluded from the region between the two filaments, resulting in an imbalance of osmotic pressure and effective attractive interactions.[18] The range and strength of such depletion interactions can be tuned by respectively changing the radius of gyration and concentration of the depletant.

At low dextran concentrations, the viruses condense into dense rod-rich nematic tactoids with ellipsoidal shape which coexist with a background isotropic suspension enriched in depleting polymer.[14,20] Within each tactoid rods lie parallel to the rod–polymer interface. Such interfaces do not exhibit significant fluctuations, indicating a very high interfacial tension. Presumably, this is because fluctuations of a liquid crystalline interface with planar anchoring are tightly coupled with the distortions of the underlying bulk liquid crystal, greatly increasing their energetic cost. Higher depletant concentrations raise the osmotic pressure of the surrounding fluid, increasing the concentration of rods within a tactoid and leading to a transition in the condensate morphology from 3D tactoids to 2D monolayers of aligned rods (Fig. 1a).[16] While quite distinct on molecular lengthscales, the continuum properties of these monolayers are identical to those of lipid bilayers, meriting the name colloidal membranes. The assembly of colloidal membranes is highly sensitive to rod monodispersity, which could explain why they have not been observed in polydisperse suspensions of synthetic rods. Furthermore, colloidal rods need to have a minimal aspect ratio to form membrane-like structures. Computer simulations indicate that this ratio is roughly equal to 20, but its precise value likely depends on the nature of the colloidal system and its underlying interactions.[15]

Complimentary optical microscopy methods have elucidated the detailed structure of colloidal membranes. Movies of

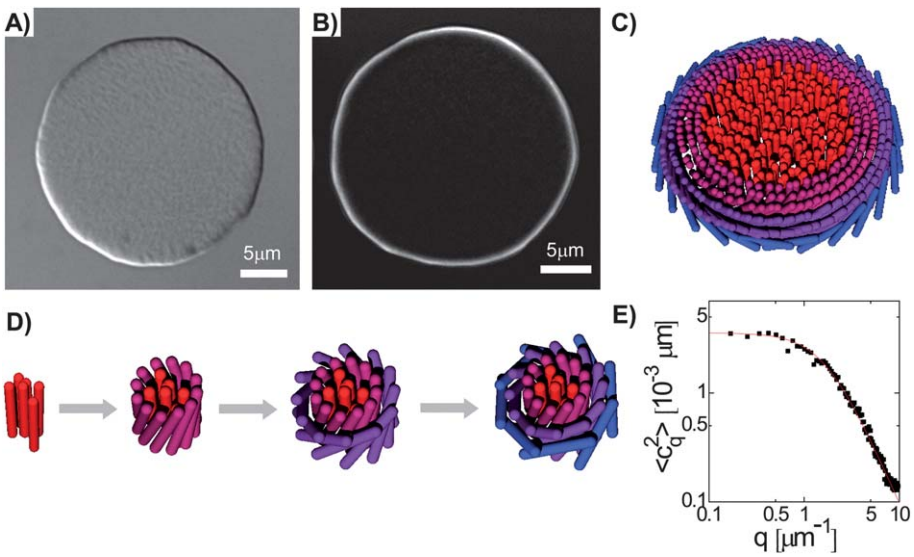

Fig. 1 The structure of colloidal membranes. (A) DIC micrograph of a colloidal membrane, viewed face-on. (B) LC-PolScope micrograph of a membrane, in which the intensity at each pixel is proportional to the magnitude of the local 2D projection of the 3D retardance vector. For rod-like virus assemblages, the retardance is proportional to the tilt angle of the rods' long axis away from the layer normal and the layer thickness. The image reveals the tilting of rods associated with the membrane's edge. (C) A schematic diagram of a colloidal membrane, showing an untilted interior and a twisted ring along the edge. The rod color indicates the magnitude of tilt, and the rod aspect ratio is reduced by an order of magnitude for visual clarity. (D) Illustration of the growth process of a monolayer composed of chiral rods which tend to tilt with respect to their neighbors. At the last frame, no further rods can be added while preserving the smectic structure of the layer and satisfying preferred chiral interactions. At this point the membrane grows by untwisting rods in the interior which raises their free energy. (E) A typical fluctuation spectrum of a colloidal membrane edge, showing the mean squared Fourier amplitudes for each spatial frequency q (black squares). The red line is a fit to the data using eqn (5). Decreased fluctuations amplitudes above $q \simeq 1\ \mu m^{-1}$ which scale as q^{-2} indicate a finite bending rigidity associated with the quasi-1D nematic phase at the membrane's edge.

membranes containing a small fraction of fluorescently labeled viruses reveal internal dynamics and indicate liquid-like organization of rods within a membrane.[16] The 2D LC-PolScope technique, in which the intensity of each pixel is proportional to the magnitude of the local retardance, reveals the average orientation of rods throughout the membrane (Fig. 1b).[21] In the interior, the membrane appears black, indicating that rods are aligned along the layer normal. By contrast, a bright band appears at the membrane's edge indicating local rod tilting. Such information suggests the membrane structure illustrated in Fig. 1c, and this hypothesis is supported by other optical and high-resolution electron microscopy techniques.[17]

The assembly pathways of 2D membranes are critically affected by the chirality of the constituent viruses, a property which can be tuned either through physical or genetic methods.[17,23–25] For chiral rods, the free energy of two parallel viruses is minimized when they are twisted with respect to one another. In practice this tilt angle is quite small, usually a fraction of a degree. The assembly of large 2D colloidal membranes is incompatible with local chiral twist as illustrated schematically in Fig. 1d. Beginning with a small aggregate of aligned rods, the membrane grows through the addition of rods which satisfy preferred chiral interactions with the initial cluster by twisting with respect to the layer normal. Further growth requires addition of more rods that are twisted with an even larger angle. As the monolayer grows in this fashion, eventually the outer rods are twisted by 90 degrees with respect to the layer normal. This melts the smectic order present in the membrane interior into a 1D nematic phase. At this point, it is impossible to grow the monolayer further while continuing to satisfy local chiral interactions. In order for the membrane to grow, the rods in the interior must locally untwist. It follows that for macroscopic membranes chiral twist penetrates only a characteristic distance into the membrane interior, which for our particular system is approximately 0.5 μm.[21] According to the deGennes analogy between Smectic-A liquid crystals and superconductors, the twist penetration lengthscale in smectic liquid crystals is analogous to the London penetration length that characterizes the interaction between superconductors and magnetic fields.[22]

Incompatibility between local chiral twist and global assembly of 2D membranes has important consequences for the interfacial tension associated with the membrane's edge. Increasing the strength of chiral interactions raises the free energy of untwisted rods in the membrane interior while simultaneously lowering the energy of edge bound rods. Therefore, chirality in effect controls the magnitude of the interfacial tension. For sufficiently chiral rods the interfacial tension approaches very small values, leading to the nucleation and growth of twisted ribbons throughout the membrane periphery.[17] In twisted ribbons essentially all rods are located in the vicinity of the twisted edge, so that such structures accommodate significantly more chiral twist than a flat 2D monolayer.

2.2 Interfacial free energy and fluctuation spectrum

A striking feature of membrane edges are their large fluctuations. These are significantly different from a typical interface where the free energy is simply proportional to the interface length, with the magnitude of the interfacial tension as the proportionality factor. As discussed previously, at the edge of colloidal membranes rods tilt, which locally melts the smectic order, inducing the formation of a quasi-1D annulus consisting of a nematic (cholesteric) phase. The elasticity of this nematic phase suppresses small-wavelength fluctuations and leads to the formation of an unconventional interface that has a finite bending rigidity. To quantitatively analyze such effects we write the free energy of a membrane's edge as:

$$F = \int \mathrm{d}x \left(\gamma \sqrt{1 + \left(\frac{\mathrm{d}y}{\mathrm{d}x}\right)^2} + \frac{1}{2}\kappa \left(\frac{\mathrm{d}^2 y}{\mathrm{d}x^2}\right)^2 \right) \quad (1)$$

where γ is the line tension, κ the bending rigidity, and the integral is evaluated over the edge contour lying in the x–y plane and parameterized by x. The first term is proportional to the interface length and is sufficient to describe conventional fluid–fluid interfaces. The second term is associated with the finite bending rigidity of the edge, and is proportional to the square of the local interfacial curvature. Based on experimental observations, we have assumed that the fluctuations of the membrane edge are small compared to the membrane radius, such that $y(x)$ is a one-to-one function and this parametrization is valid. If we define the tangent angle $\tan(\theta(x)) = \frac{\mathrm{d}y}{\mathrm{d}x}$, and assume that the fluctuations about a flat interface oriented along the x-axis are small, we can rewrite eqn (1) as:

$$\Delta F = \int \mathrm{d}x \frac{1}{2} \left(\gamma \theta^2(x) + \kappa \left(\frac{\mathrm{d}\theta(x)}{\mathrm{d}x}\right)^2 \right) \quad (2)$$

where $\Delta F = F - F_{\mathrm{flat}}$ is the free energy difference between an instantaneous interfacial conformation and a flat interface. To determine the effect of the bending energy term on membrane edge fluctuations, we write down the Fourier series for θ:

$$\theta(x) = \sqrt{\frac{2}{L_{\mathrm{edge}}}} \sum_q \left(a_q \cos(qx) + b_q \sin(qx) \right) \quad (3)$$

where q is the spatial wavevector conjugate to the coordinate x, a_q and b_q are the cosine and sine Fourier coefficients at wavevector q, respectively, and L_{edge} is the contour length of the membrane edge. Rewriting eqn (2) in Fourier space yields:

$$\Delta F = \sum_q \frac{1}{2} \left(\gamma + \kappa q^2 \right) \left({a_q}^2 + {b_q}^2 \right) \quad (4)$$

The equipartition theorem states that each quadratic degree of freedom has on average $\frac{1}{2} K_{\mathrm{B}} T$ to thermal energy. Plugging this result into eqn (4) yields:

$$\left\langle {c_q}^2 \right\rangle = \frac{K_{\mathrm{B}} T}{\gamma + \kappa q^2} \quad (5)$$

where $\langle {c_q}^2 \rangle = \frac{1}{2} \langle {a_q}^2 + {b_q}^2 \rangle$ are the mean squared Fourier amplitudes at each wavevector q. In the absence of a bending energy term, these amplitudes are constant for all wavelengths. With the addition of this term, small wavelength fluctuations become energetic costly, so that constant amplitudes at low q

give way to q^{-2} scaling above a characteristic crossover at wavevector $\sqrt{\gamma/\kappa}$. Thus finite bending rigidity suppresses small-wavelength fluctuations, effectively smoothing out the interface. We have previously shown that this simple model of a fluid interface with finite bending rigidity quantitatively describes experimental fluctuation spectra for colloidal membrane edges (Fig. 1e).[17] We next seek to modify the properties of such an interface through addition of appropriately chosen edge-active agents.

3 Experimental results

3.1 Methods

fd virus was grown in host *E. coli* cells and purified to high monodispersity using previously reported methods.[16] F-Actin was purified and polymerized as previously described.[26] G-Actin stocks labeled with Alexa-488 (Molecular Probes) and NHS–PEG4–biotin (Thermo Scientific) were mixed at a ratio of 2 : 1, respectively, polymerized in high salt suspension and subsequently stabilized with phalloidin (Invitrogen). Bacterial flagella were isolated from *Salmonella typhimurium* strains SJW 1103 (wild-type, curly morphology) and 1660 (straight morphology) as previously described.[27] Once polymerized, flagella were co-labeled with a mixture of rhodamine dye (Invitrogen) and NHS–PEG4–biotin. 1 μm silica microspheres (Bangs Laboratories) were coated with streptavidin in order to bind and translate biotin-labeled filaments.

Membrane-forming samples were prepared at 0.5 mg mL^{-1} *fd*, 45 mg mL^{-1} dextran (M_w 500 000, Sigma) in 20 mM Tris, 125 mM NaCl, pH 8.1. Glass coverslides (VWR) and coverslips (GoldSeal) were coated with an acrylamide brush to prevent sticking to the surface.[26] Unstretched parafilm was used as a spacer between the coverslide and coverslip. In preparing samples with actin or flagella filaments, the following sample preparation procedure was employed to prevent filament degradation while colloidal membranes formed. The spacers were placed in order to form an "H-shaped" channel with four openings. The channel was then completely filled with the virus solution, and two openings were sealed with UV-sensitive optical glue (Norland Products). The sample was stored in a saturated water vapor environment to prevent evaporation through the unsealed openings, thus allowing sufficient time for assembly of large membranes. After approximately 24 hours, a solution containing actin/flagella filaments, glass beads, and dextran was flowed through an unsealed opening, and the sample was sealed. For experiments involving the temperature-induced membrane–ribbon transition, experimental difficulties arise in achieving the transition using the above sample preparation technique, as the polymer concentration must be finely tuned. Therefore we utilized a "T-shaped" chamber design, and flowed in all the components at once. Additionally, although not essential, the presence of 0.5% Triton X-100 in the final solution expands the range of system parameters over which the membrane–ribbon transition is observed, and was utilized to facilitate the experiment.

We used an inverted microscope equipped with DIC, dark-field, and fluorescence imaging modules (TE-2000, Nikon). A 100× plan fluor oil immersion objective with numerical aperture variable between 0.7 and 1.3 (Nikon) was used. Fluorescence images were taken using an X-Cite high intensity mercury–halide light source (Lumen Dynamics) and dichroic filter cubes for both Alexa-488 and rhodamine dyes (Chroma). Images were captured using an Andor Clara monochrome cooled CCD camera. For dual-channel data, images for each channel were taken sequentially about 200 ms apart by using a VMM-D3 multi-channel shutter controller (Uniblitz) and subsequently overlayed. Optical trapping was performed by slightly overfilling the rear aperture of the objective with the beam of a 4 Watt Nd:YAG laser (Coherent). Sample temperature was varied using a peltier device as previously described.[17] Edge fluctuation data was analyzed using homemade IDL procedures.

3.2 Tuning the bending rigidity of membrane's edge

We seek to identify edge-active agents that control the magnitude of the bending rigidity κ of the colloidal membrane edge. To accomplish this goal we utilize the fact that near the membrane's edge, the smectic ordering of the membrane bulk melts into a nematic-like phase. Filaments whose length exactly matches the thickness of the colloidal membrane will preferentially partition into the membrane interior. However, longer filaments will protrude from the membrane, significantly decreasing the excluded volume available to the polymers and raising the overall free energy of the system. Similarly, such filaments are also insoluble in the bulk depletant phase which envelops the colloidal membrane. Being insoluble in both the 2D bulk membrane phase and the 3D isotropic polymer phase, long filaments will preferentially partition into the 1D nematic phase located at the membrane's edge. This scenario leads to a new type of "geometrical surfactant" that preferentially adheres to the membrane's edge not due to specific energetic interactions, but instead acts due to geometrical constraints imposed by a specific self-assembly architecture.

To test this hypothesis we have added a low volume fraction of long semi-flexible filaments to colloidal membranes. We have used two types of biological filaments: F-actin and bacterial flagella. Detailed analysis of fluctuations reveals that the persistence length of phalloidin-stabilized actin filaments is 17.8 μm,[28] corresponding to a bending rigidity of $17.8K_BT$ μm. Literature reports for the persistence length of flagella range from 250 μm to 25 mm,[29,30] with the most recent measurement being $L_p \simeq 850$ μm.[31] A suspension of highly purified flagella or F-actin contains many filaments that are tens of microns in length, a highly desirable feature for our experiments.

Mixing F-actin with colloidal membranes leads to adsorption of essentially all filaments to the membranes' edges, although the number adhered per membrane exhibits large spatial variations and is difficult to measure, precluding quantitative analysis. We have therefore developed an experimental procedure that allows for more control. Specifically, we use optical tweezers to bind a streptavidin-coated bead to one end of a biotin labeled filament. Subsequently, such a filament is translated using an optical tweezer to the vicinity of a membrane, where it spontaneously binds to the edge. This procedure allows us to

sequentially add a predetermined number of filaments at a well-defined spatial position along a membrane's edge. Fig. 2a shows a dual-channel image of several actin filaments adhered to a single locus on a membrane interface.

Using the above scheme we first estimate the binding energy of an isolated F-actin filament to the membrane's edge. A single filament is partially adsorbed onto the interface at one end, while the other end containing a microsphere is held at a fixed distance away from the membrane using an optical trap (Fig. 2b). The configuration of such a partially desorbed filament will depend on both the filament's persistence length and the adsorption strength. For stiff filaments or weak adhesion energies the filament curvature at the point where it desorbs from the membrane's edge will be quite small. In the opposite limit of floppy filaments or strong adhesion, the filament will heavily bend and desorb over a small characteristic lengthscale. To quantitatively analyze such images we assume that the filament conforms exactly to the membrane interface over a distance L_0, and then connects straight to the trapped bead located a distance h away from the membrane. In between these two regimes, we approximate the contour of the filament as a quarter circle of radius R. The membrane–filament overlap length is then given by:

$$L_0 = L - \left(\frac{\pi}{2} - 1\right)R - h \tag{6}$$

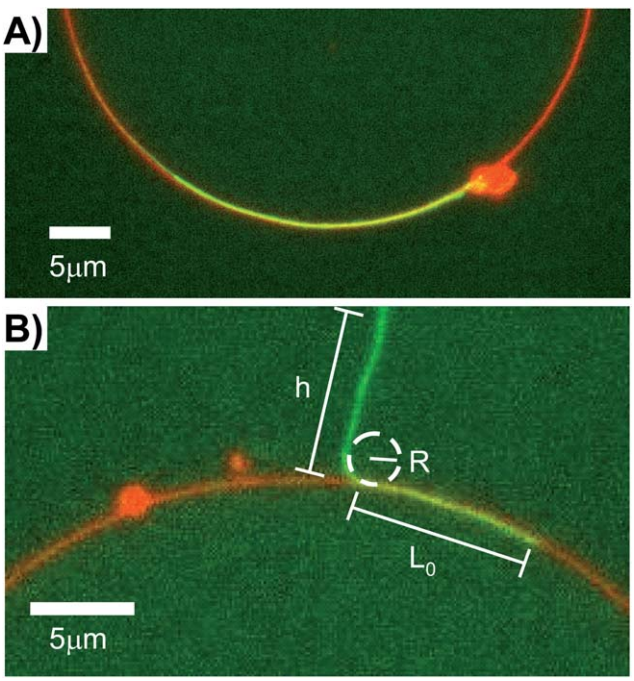

Fig. 2 Actin filament adsorption onto the membrane edge. (A) A dual-channel darkfield (red) and fluorescence (green) micrograph of a bundle of several actin filaments adsorbed onto the edge of a colloidal membrane. The bright spot on one edge indicates a cluster of microspheres used to bring the filaments into membrane proximity. (B) A dual-channel image showing the configuration of partially adsorbed actin filament that is used to estimate edge adhesion. A single actin filament is partially adsorbed from a membrane by holding one end a fixed distance from the interface using an optical trap. The length of the adsorbed segment is L_0, the length of free filament is h, and the radius of the quarter-circle joining the bound and unbound sections is R.

where L is the total length of the filament. The total energy of a partially adsorbed filament is given by:

$$E = -\lambda L_0 + \frac{\pi}{2}\frac{\kappa}{R} + \frac{\kappa}{{R_m}^2}L_0 \tag{7}$$

where λ is the binding energy of a filament to the membrane's edge per unit length, κ is the bending rigidity of an actin filament and R_m is the radius of the membrane onto which the filament is adsorbed. The second and third terms are associated with the energetic cost of bending the actin filament near the desorption point and at the membrane's edge, respectively. Minimizing the above expression with respect to R yields:

$$\lambda = \frac{\frac{\pi}{2}}{\frac{\pi}{2} - 1}\frac{\kappa}{{R^*}^2} + \frac{\kappa}{{R_m}^2} \tag{8}$$

Using experimentally measured values of R_m, R^* and κ yields $\lambda = 21.8 K_B T/\mu m$. This result is consistent with the quick "zipping up" of the actin filament once partially adsorbed, as the binding energy dominates thermal fluctuations. Previously, we have used a similar analysis to estimate the binding energy between a pair of actin filaments.[26] Such experiments yield adhesion energies that are comparable to our present result.

To measure the effect of actin's presence on interfacial properties, we bind a long actin filament to a particular location on the membrane's periphery. Subsequently, we capture five independent sets of data, each containing one thousand uncorrelated images of a fluctuating membrane. The region of the edge where the filament is adsorbed is digitized and analyzed as described previously.[17] We repeat the above measurement for different numbers of filaments adhered to the same region. The fluctuation spectra obtained using this procedure are shown in Fig. 3a. We fit the spectra to eqn (5) and extract the dependence of the bending rigidity κ on the number of filaments embedded into the membrane's edge. Increasing the number of filaments significantly influences the bending rigidity of the interface. For our experimental conditions the bending rigidity of the bare edge is about $200 K_B T/\mu m$, and increases steadily to about $400 K_B T/\mu m$ for an edge which contains six actin filaments (Fig. 3b). We note that for low numbers of filaments, there is a peak in fluctuation amplitudes at around $q = 1\ \mu m^{-1}$ which is associated with the onset of a transition to twisted ribbons.[17] This peak skews the fit near the transition from the flat regime to the q^{-2} regime, which is crucial in determining the value of κ. This peak also prevents accurate determination of the magnitude of the line tension γ from the fit. Statistical weighting ($w_i = 1/y_i$) was implemented in the fit to eqn (5) in order to produce a more accurate fit in the q^{-2} regime and determine κ more accurately.

The effective bending rigidity of a filamentous bundle is highly sensitive to the nature of the interfilament sliding interactions.[32,33] For structures in which filaments freely slide past each other the effective bundle bending rigidity will increase linearly with number of filaments. In comparison, filaments that are rigidly cross-linked will assemble into bundles whose effective bending rigidity grows as the number

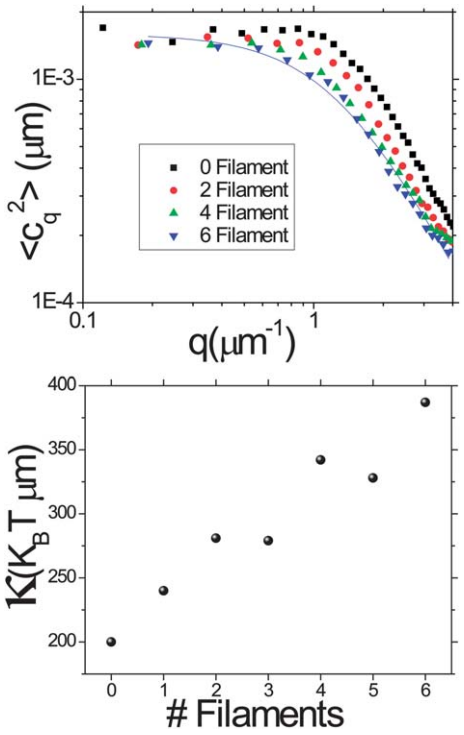

Fig. 3 Fluctuation analysis of actin-bound membranes. (A) Fluctuation spectra showing the mean square Fourier amplitudes $\langle c_q^2 \rangle$ *vs.* spatial wavevector q for differing numbers of actin filaments adsorbed onto the membrane edge. The analysis is performed only on the region of the edge on which the filaments are adsorbed. The shift of the crossover from q^0 to q^{-2} scaling to lower q values indicates an increase in bending rigidity with increasing filament number. A fit of eqn (5) to the six-filament data is shown. (B) The binding energy κ extracted from the fluctuation spectra plotted as a function of filament number.

of filaments squared. The coupling of actin filaments to each other and to the background nematic seems to falls closer to the limit of freely sliding filaments for two reasons. First, we find that the effective bending rigidity scales linearly with the number of filaments, indicating freely sliding interactions. Second, assuming purely additive interactions we would expect that six adsorbed filaments increase bending rigidity by about $100K_BT/\mu m$. This is about half of experimentally measured effect ($200K_BT/\mu m$) indicating that there is perhaps weak viscoelasticity associated with interfilament sliding.

The increased bending rigidity due to the presence of actin filaments at the membrane edge can be strikingly visualized by inducing a chirality-driven membrane-to-ribbon polymorphic transition. As described previously, increasing the strength of chirality in the constituent rods decreases the edge line tension, leading to critically large fluctuations and the nucleation of twisted ribbons throughout the monolayer's edge. We repeat this experiment with a membrane whose edge is partially covered with an actin filament bundle (Fig. 4, ESI Movie 1†). As chirality is increased (by reducing the sample temperature), fluctuations of the edge in contact with the actin filament are suppressed due to the locally increased bending rigidity, preventing local nucleation of ribbons. In contrast, on the bare edge, ribbons nucleate and grow uninhibited. Thus edgeactant-induced modification of membrane bending rigidity leads to local control over the kinetics of this transition.

To demonstrate the ability of diverse filaments to act as edge-modifying agents, we repeated the previously described experiments with straight bacterial flagella. These filaments have similar dimensions to actin, but are significantly more rigid.

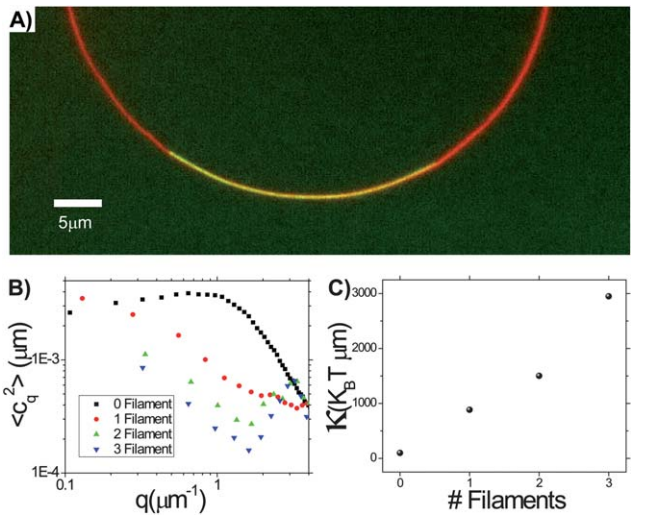

Fig. 5 Fluctuation analysis of flagella-bound membranes. (A) A dual-view darkfield-fluorescence image of a single flagellum (green) bound to a membrane edge (red). (B) Fluctuation spectra of a membrane edge with varying number of bound flagella. (C) The bending rigidity κ *vs.* flagella filament number. The increase in bending rigidity per filament is much larger than in the actin case because the flagella are much stiffer. The increase in fluctuation amplitudes above $\sim q = 1.5$ μm could be due to decoupling of the filament from the membrane edge at those wavelengths.

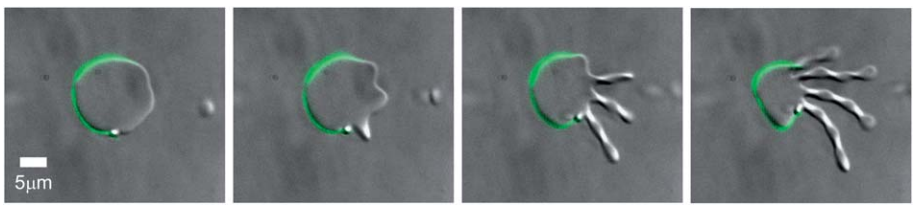

Fig. 4 Adsorbed filaments locally suppress the membrane–ribbon transition. A dual channel time sequence of a membrane (DIC, gray) whose edge is partially covered with an actin filament bundle (fluorescence, green). The membrane undergoes a chirality-induced transition into twisted ribbons. This polymorphic transition is induced by increasing the strength of chiral interactions by reducing temperature from $T = 55$ °C to $T = 10$ °C. Fluctuations of the edge near the actin filament are suppressed due to increased bending rigidity; consequently ribbons only nucleate on the filament-free section of the membrane interface. The total time lapse between the first and last image is one minute.

Similarly to actin filaments, we find that flagella preferentially incorporate at the membrane's edge (Fig. 5a). Following the experimental procedures described, we measured the fluctuation spectrum for a membrane's edge which contains a varying number of adsorbed flagella (Fig. 5b, ESI Movie 2†). In this case, fluctuations are suppressed even at very low q, indicating a much higher bending rigidity for flagella than for actin filaments. We find that the bending rigidity goes up from about $100K_BT/\mu m$ for a bare edge to over $3000K_BT/\mu m$ for an edge with a three-bound flagella (Fig. 5c). Assuming κ compounds additively, we would arrive at a value of $1000K_BT/\mu m$ for a flagellum, or a persistence length of 1 mm, which is within the range reported in literature. Again there is significant error in the fit, especially for higher filament numbers, for which the low-q plateau is pushed below the experimentally measurable range.

It is also found that the effect of filament binding on the shape of the membrane edge varies depending on the concentration of depleting polymer. There are three main forces governing the shape of an edge with an adsorbed filament: (1) the edge line tension, (2) the edge bending rigidity, and (3) the filament bending rigidity. At relatively high polymer concentration, as was used in the fluctuation analysis experiments, the interfacial tension of the monolayer dominates, forcing the filament to conform to the edge shape as shown in Fig. 3a. At lower line tension, for stiff filaments such as flagella, the filament bending energy dominates, resulting in alteration of the shape of the membrane edge. Fig. 6a shows a membrane locally distorted from a circular shape by a straight flagellum. Edgeactants with complex geometries result in more interesting shape changes. Fig. 6b and c show a membrane edge locally curved to conform to the shape of a curly flagellum, forming a rippled edge. Thus osmotic pressure provides a knob by which to tune the degree to which a geometrical surfactant dominates the membrane interfacial conformation.

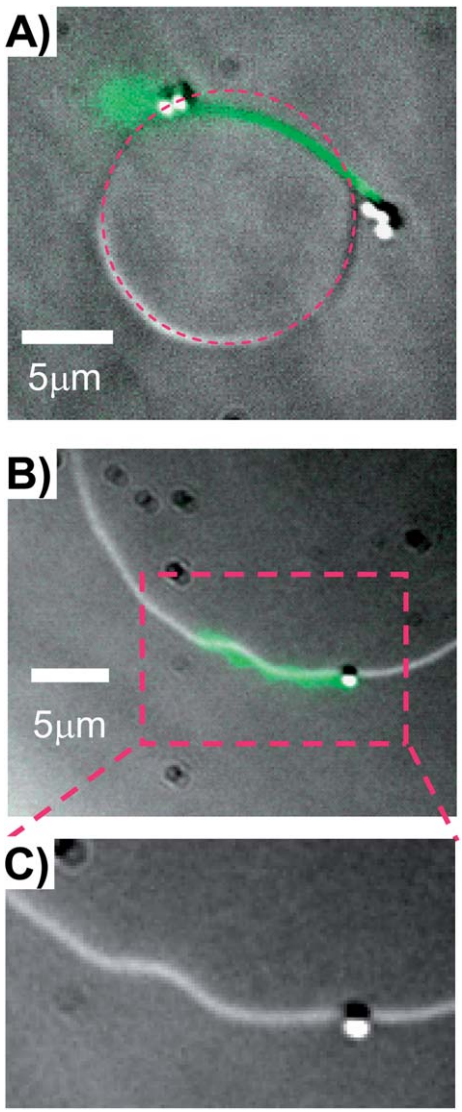

Fig. 6 Flagella-induced deformations of the monolayer edge. (A) A dual-channel image of a fluorescent flagellum (green) on a membrane edge (gray) viewed with DIC. The pink dot-dashed circle outlines the equilibrium shape of the same membrane before the attachment of the flagellum, showing that the membrane edge is locally deformed by the filament. (B) A curly flagellum adsorbed onto a membrane interface. (C) A zoom in on the DIC channel of the dashed pink box in (B) showing the local conformation of the membrane edge to the shape of the flagellum.

4 Conclusion

An edge of a colloidal membrane has a complex partially ordered structure characterized by the presence of a quasi-1D nematic phase. Such a structure leads to complex fluctuations which in the long wavelength limits are governed by the one-dimensional interfacial tension. At small wavelengths, the 1D nematic phase suppresses the fluctuations, effectively smoothing out the edge. We have previously demonstrated that it is possible to use chirality of the constituent rods to tune the amplitudes of large wavelength fluctuations of a membrane's edge. Here we have demonstrated a versatile method for controlling the portion of the fluctuation spectrum controlled by bending rigidity. The addition of edgeactants such as actin and flagella filaments tunes the local rigidity of the membrane edge in a controllable and predictable way – stiffer molecules result in stiffer interfaces. The colloidal membrane system described here is an example of how geometry and the frustration of constituent rods can lead to unexpected and non-trivial self-assembly pathways.

Acknowledgements

This work was supported by US National Science Foundation through grants DMR-0955776, MRI-0923057 and MRSEC-0820492 and Brandeis MRSEC optical microscopic facility.

References

1 S. Safran, *Statistical Thermodynamics of Surface, Interfaces, and Membranes*, Addison Wesley, 1994.
2 C. Fradin, *et al.*, *Nature*, 2000, **403**, 871–874.
3 D. G. A. L. Aarts, M. Schmidt and H. N. W. Lekkerkerker, *Science*, 2004, **304**, 847–850.

4 D. G. A. L. Aarts, R. P. A. Dullens and H. N. W. Lekkerkerker, *New J. Phys.*, 2005, **7**, 40.
5 W. L. Chen and D. G. Gray, *Langmuir*, 2002, **18**, 633–637.
6 R. H. J. Otten and P. van der Schoot, *Langmuir*, 2009, **25**, 2427–2436.
7 K. Shundyak and R. van Roij, *Phys. Rev. E: Stat. Phys., Plasmas, Fluids, Relat. Interdiscip. Top.*, 2003, **68**, 061703.
8 R. L. C. Vink and T. Schilling, *Phys. Rev. E: Stat., Nonlinear, Soft Matter Phys.*, 2005, **71**, 051716.
9 S. Wolfsheimer, C. Tanase, K. Shundyak, R. van Roij and T. Schilling, *Phys. Rev. E: Stat., Nonlinear, Soft Matter Phys.*, 2006, **73**, 061703.
10 Z. Y. Chen and J. Noolandi, *Phys. Rev. A: At., Mol., Opt. Phys.*, 1992, **45**, 2389–2392.
11 M. Dijkstra, R. van Roij and R. Evans, *Phys. Rev. E: Stat. Phys., Plasmas, Fluids, Relat. Interdiscip. Top.*, 2001, **63**, 051703.
12 D. van der Beek, *et al.*, *Phys. Rev. Lett.*, 2006, **97**, 087801.
13 N. Puech, E. Grelet, P. Poulin, C. Blanc and P. van der Schoot, *Phys. Rev. E: Stat., Nonlinear, Soft Matter Phys.*, 2010, **82**, 020702.
14 Z. Dogic, *Phys. Rev. Lett.*, 2003, **91**, 165701.
15 Y. Yang, E. Barry, Z. Dogic and M. F. Hagan, *Soft Matter*, 2012, **8**, 707–714.
16 E. Barry and Z. Dogic, *Proc. Natl. Acad. Sci. U. S. A.*, 2010, **107**, 10348–10353.
17 T. Gibaud, E. Barry, M. J. Zakhary, M. Henglin, A. Ward, Y. Yang, C. Berciu, R. Oldenbourg, M. F. Hagan, D. Nicastro, R. B. Meyer and Z. Dogic, *Nature*, 2012, **481**, 348–351.
18 S. Asakura and F. Oosawa, *J. Chem. Phys.*, 1954, **22**, 1255.
19 E. Nordmeier, *J. Phys. Chem.*, 1954, **97**, 5770.
20 M. P. Lettinga, K. Kang, A. Imhof, D. Derks and J. K. G. Dhont, *J. Phys.: Condens. Matter*, 2005, **17**, S3609–S3618.
21 E. Barry, Z. Dogic, R. B. Meyer, R. A. Pelcovits and R. Oldenbourg, *J. Phys. Chem. B*, 2009, **113**, 3910–3913.
22 P. G. DeGennes, *Solid State Commun.*, 1972, **10**, 753.
23 E. Grelet and S. Fraden, *Phys. Rev. Lett.*, 2003, **90**, 198302.
24 F. Tombolato, A. Ferrarini and E. Grelet, *Phys. Rev. Lett.*, 2006, **96**, 258302.
25 E. Barry, D. Beller and Z. Dogic, *Soft Matter*, 2009, **5**, 2563.
26 A. W. C. Lau, A. Prasad and Z. Dogic, *Europhys. Lett.*, 2009, **87**, 48006.
27 E. Barry, Z. Hensel, Z. Dogic, M. Schribak and R. Oldenbourg, *Phys. Rev. Lett.*, 2006, **96**, 018305.
28 F. Gittes, B. Mickey, J. Nettleton and J. Howard, *J. Cell Biol.*, 1993, **120**, 923.
29 S. Fujime, M. Maruyama and S. Asakura, *J. Mol. Biol.*, 1972, **68**, 347.
30 H. Hoshikawa and R. Kamiya, *Biophys. Chem.*, 1985, **22**, 159.
31 N. C. Darnton and H. C. Berg, *Biophys. J.*, 2007, **92**, 2230.
32 M. M. A. E. Claessens, *et al.*, *Nat. Mater.*, 2006, **5**, 748.
33 C. Heussinger, M. Bathe and E. Frey, *Phys. Rev. Lett.*, 2007, **99**, 048101.